Novel Sensorless Control Algorithm for SyR Machines Based on Low Speed Active Flux

Novel Sensorless Control Algorithm for SyR Machines Based on Low Speed Active Flux

Paolo Pescetto
Politecnico di Torino
Department of energy "Galileo Ferraris"
Torino, Italy
paolo.pescetto@polito.it

Arzhang Yousefi-Talouki
ABB Oy
Helsinky, Finland
arzhang.yousefitalouki@fi.abb.com

Gianmario Pellegrino
Politecnico di Torino
Department of energy "Galileo Ferraris"
Torino, Italy
gianmario.pellegrino@polito.it

***Abstract*—This work deals with encoderless control of synchronous reluctance machines at low and zero speed. The algorithm is based on active flux method, often exploited to retrieve the rotor position at sufficiently high speed. being a model based technique, the active flux commonly fails when the speed is too low due to lack of back-emf and so low signal-to-noise ratio, and is impossible at standstill. The active flux concept is now generalized and extended to cover also the low speed range, where the control is enhanced by HF voltage injection. The fundamental and HF machine models are decoupled, permitting to exploit the model based algorithm also at standstill. The proposed technique was experimentally tested in a 1.1 kW motor prototype with promising results.**

***Index Terms*—Synchronous reluctance machines, sensorless control, active flux, low speed, saliency based.**

I. Introduction

Synchronous Reluctance Motor (SyRM) drives are becoming an interesting solution for replacing Induction Motors (IM) in several variable speed applications. In particular, SyRMs do not present rotor current, so joule losses are only present in the stator, leading to higher efficiency. If compared with the other synchronous machines, the absence of Permanent Magnets (PM) reduces the manufacturing costs, with often higher mechanical robustness. Moreover, the inherently anisotropic rotor structure of SyRMs makes them appealing for saliency based encoderless control.

Sensorless control strategies are commonly divided in two main categories. The machine equations can be manipulated to retrieve the rotor position from the reference voltages and measured currents [1]–[4] (model based approach). These techniques usually require to exploit the back-EMF of the machine, and they work very well when the rotor speed is sufficiently high. At low speed, the back-EMF are reduced, so eventual inaccuracies in parameters estimation (e.g. stator resistance) or in compensating the inverter voltage drop become more relevant in percentage, deeply affecting the reliability of position estimation. At standstill, the back-EMF are null, so model based approach becomes impossible.

For this reason, sensorless control at low speed commonly adopts saliency based position tracking, where an High Frequency (HF) signal (voltage, current or flux) is injected and the HF machine response is manipulated to retrieve the rotor position. The literature presents many examples of saliency based algorithms [5]–[7], being the difference between them mostly the type of injected and demodulated signal and the demodulation algorithm.

Saliency based techniques are rarely adopted at medium-high speed due to several reasons. The injection of the HF signal reduces the available voltage, possibly affecting the control performances. Also, the current measurement delay becomes more relevant when the speed increases, influencing the position estimation. Finally, the HF signal produces additional iron losses and is unnecessary when the speed is sufficiently high so that model based algorithms can be exploited. The literature presents several works combining model based and saliency based techniques in hybrid sensorless algorithms [1]–[3], [8], [9].

Among the model based techniques, the Active Flux (AF) concept was proposed for the first time in [10] and then followed by other Authors like [1], [8], [9]. The principle is to turn a salient machine in an equivalent isotropic one. This method resulted accurate at medium-high speed, but, being model based, it could not be exploited at low speed and standstill.

In this work, the AF concept is generalized and extended to cover the low speed range. In particular, a sinusoidal HF voltage signal is injected, while the HF current response is demodulated. These two signal are combined to extract the HF component of the active flux vector (HF-AF). A novel strategy is also proposed to retrieve the rotor position from the HF-AF vector. The proposed technique, experimentally tested, resulted capable of accurate and robust position estimation even at standstill, i.e. the most demanding condition.

II. SyR Machine Model

A. Fundamental Model

The SyR machine is modeled in rotating dq reference frame, synchronous with the rotor, where d axis is intended as the direction of maximum inductance:

$$\boldsymbol{v}_{\mathrm{dq}} = R_{\mathrm{s}}\boldsymbol{i}_{\mathrm{dq}} + \frac{\mathrm{d}\boldsymbol{\lambda}_{\mathrm{dq}}}{\mathrm{d}t} + \omega\mathbf{J}\boldsymbol{\lambda}_{\mathrm{dq}} \tag{1}$$

where bold symbols indicate vector quantities and $\mathbf{J}$ is the imaginary matrix:

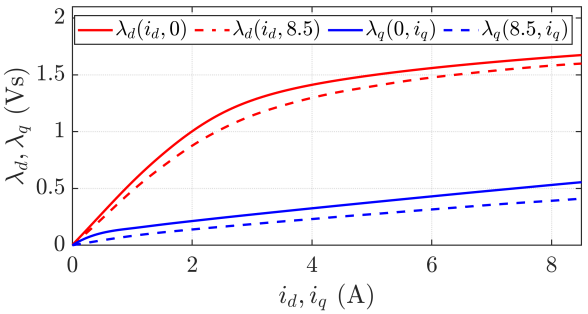

Fig. 1. Flux maps of the motor under test.

$$\mathbf{J} = \begin{bmatrix} 0 & -1 \\ 1 & 0 \end{bmatrix} \tag{2}$$

The relationship between stator currents and flux linkages is highly non-linear because of magnetic saturation. In particular, the flux in each axis depends on its own current (self-saturation) and on the current in the perpendicular direction (cross-saturation or cross-coupling).

$$\begin{cases} \lambda_\mathrm{d} &= \lambda_\mathrm{d}\left(i_\mathrm{d}, i_\mathrm{q}\right) \\ \lambda_\mathrm{q} &= \lambda_\mathrm{q}\left(i_\mathrm{d}, i_\mathrm{q}\right) \end{cases} \tag{3}$$

This non-linear relationship, commonly called flux maps, can be either retrieved from Finite Element Analysis (if available at machine design stage) [11] measured by constant speed tests [12], offline tests [13] or self-commissioning algorithms [14]–[16]. The flux maps of the motor under test are reported in Fig. 1. For machine analysis purpose, it is convenient to define the apparent inductances in dq axes:

$$L_\mathrm{d}\left(i_\mathrm{d}, i_\mathrm{q}\right) = \frac{\lambda_\mathrm{d}}{i_\mathrm{d}} \qquad L_\mathrm{q}\left(i_\mathrm{d}, i_\mathrm{q}\right) = \frac{\lambda_\mathrm{q}}{i_\mathrm{q}} \tag{4}$$

Each inductance is a function of the working point because of magnetic saturation. The cross-coupling effect is taken into account considering the variability of $\boldsymbol{\lambda}_\mathrm{dq}$ with both the current components.

B. HF Model

The HF model of the SyR machine is valid when dealing with HF injection, as common for low speed, saliency based sensorless control. In this case, the resistive voltage drop and the motional term in (1) are negligible respect to the flux derivative:

$$\boldsymbol{v}_\mathrm{dq}^\mathrm{h} = \frac{\mathrm{d}\boldsymbol{\lambda}_\mathrm{dq}^\mathrm{h}}{\mathrm{d}t} \approx \frac{\mathrm{d}\boldsymbol{\lambda}_\mathrm{dq}}{\mathrm{d}t} \tag{5}$$

where the superscript h stands for HF component. It results convenient to define the incremental inductances as the derivative of the flux respect to the current components:

$$l_\mathrm{d}\left(i_\mathrm{d}, i_\mathrm{q}\right) = \frac{\partial \lambda_\mathrm{d}}{\partial i_\mathrm{d}} \qquad l_\mathrm{dq}\left(i_\mathrm{d}, i_\mathrm{q}\right) = \frac{\partial \lambda_\mathrm{d}}{\partial i_\mathrm{q}} \tag{6a}$$

$$l_\mathrm{q}\left(i_\mathrm{d}, i_\mathrm{q}\right) = \frac{\partial \lambda_\mathrm{q}}{\partial i_\mathrm{q}} \qquad l_\mathrm{qd}\left(i_\mathrm{d}, i_\mathrm{q}\right) = \frac{\partial \lambda_\mathrm{q}}{\partial i_\mathrm{d}} \tag{6b}$$

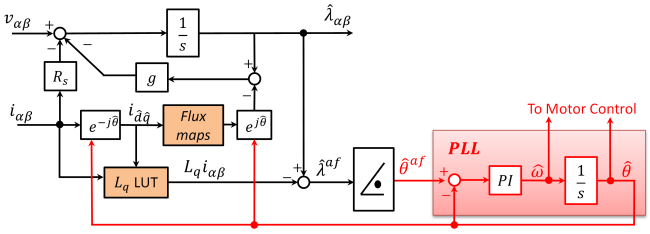

Fig. 2. Block diagram of the model based AF flux and position observer.

The two cross terms l_dq and l_qd are not null because of cross-saturation effect. The principle of energy conservation imposes the reciprocity condition $l_\mathrm{dq} = l_\mathrm{qd}$. From the first order Taylor expansion of (3), the relationship between HF current and flux component is given by:

$$\begin{cases} \lambda_\mathrm{d}^\mathrm{h}\left(i_\mathrm{d}, i_\mathrm{q}\right) &= l_\mathrm{d} i_\mathrm{d}^\mathrm{h} + l_\mathrm{dq} i_\mathrm{q}^\mathrm{h} &\approx l_\mathrm{d} i_\mathrm{d}^\mathrm{h} \\ \lambda_\mathrm{q}^\mathrm{h}\left(i_\mathrm{d}, i_\mathrm{q}\right) &= l_\mathrm{qd} i_\mathrm{d}^\mathrm{h} + l_\mathrm{q} i_\mathrm{q}^\mathrm{h} &\approx l_\mathrm{q} i_\mathrm{q}^\mathrm{h} \end{cases} \tag{7}$$

The cross-saturation effect will be neglected in the rest of the paper for sake of simplicity. This will cause a steady state position estimation error in the sensorless control, as will be discussed later. This error resulted experimentally small enough to obtain an accurate sensorless control. Anyway, the compensation of this term is currently under investigation.

III. Active Flux Concept

A. Background: Fundamental Component

The idea behind AF concept it is to turn an anisotropic ac machine into an equivalent non-salient one, and track the obtained active flux phase angle to obtain the rotor position. To explain this concept, the magnetic model of the machine must be written in terms of apparent inductances as in (4). The definition of AF vector is:

$$\boldsymbol{\lambda}^\mathrm{af} = \boldsymbol{\lambda} - L_\mathrm{q}\boldsymbol{i} \tag{8}$$

where the stator flux vector $\boldsymbol{\lambda}$ and current $\boldsymbol{i}$ can be expressed either in stator or rotor reference frame. For a SyR machine, exploiting complex representation of the vector quantities, (8) turns to be:

$$\begin{aligned} \boldsymbol{\lambda}^\mathrm{af} &= \lambda_\mathrm{d} + j\lambda_\mathrm{q} - L_\mathrm{q}\left(i_\mathrm{d} + j i_\mathrm{q}\right) \\ &= L_\mathrm{d} i_\mathrm{d} + j L_\mathrm{q} i_\mathrm{q} - L_\mathrm{q}\left(i_\mathrm{d} + j i_\mathrm{q}\right) \\ &= \left(L_\mathrm{d} - L_\mathrm{q}\right) i_\mathrm{d} \end{aligned} \tag{9}$$

Therefore, the q component of the vector $\boldsymbol{\lambda}^\mathrm{af}$ is null, i.e. $\boldsymbol{\lambda}^\mathrm{af}$ is aligned with the d axis. So, $\boldsymbol{\lambda}^\mathrm{af}$ can be conveniently calculated in $\alpha\beta$ reference frame, and its phase corresponds to the rotor position, as illustrated in Fig. 3(a):

$$\begin{cases} \sin\hat{\theta}^\mathrm{af} &= \dfrac{\boldsymbol{\lambda}_\beta^\mathrm{af}}{\left|\boldsymbol{\lambda}^\mathrm{af}\right|} &= \dfrac{\hat{\lambda}_\beta - L_\mathrm{q} i_\beta}{\left|\boldsymbol{\lambda}^\mathrm{af}\right|} \\ \cos\hat{\theta}^\mathrm{af} &= \dfrac{\boldsymbol{\lambda}_\alpha^\mathrm{af}}{\left|\boldsymbol{\lambda}^\mathrm{af}\right|} &= \dfrac{\hat{\lambda}_\alpha - L_\mathrm{q} i_\alpha}{\left|\boldsymbol{\lambda}^\mathrm{af}\right|} \end{cases} \tag{10}$$

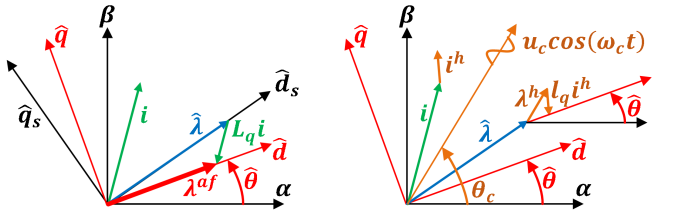

(a) (b)

Fig. 3. Visual representation of AF concept. (a) Fundamental model, (b) HF component.

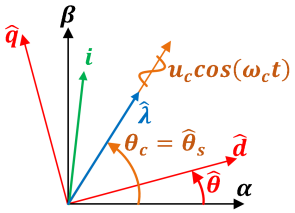

Fig. 4. Proposed implementation of HF-AF.

This position estimation can be either directly used for dq axes definition or sent to a PLL for more robust position and speed extraction, at the cost of limiting the bandwidth of position tracking. Fig. 2 illustrates the resulting active flux observer. Normally, a fixed L_q is used. In [1], the value of L_q was online varied, improving the reliability of the estimated position.

It should be noted that, in the original formulation of [10], the AF concept was written for Internal Permanent Magnet (IPM) machines, so the convention of the dq coordinates (d axis on the minimum inductance direction) was reversed respect to the one adopted for SyRM. Also in this case, despite the different meaning of the terms, the vector $\boldsymbol{\lambda}^{\mathrm{af}}$ still drops on the d axis.

B. Extension to HF Component

The main idea of this work is to extend the AF concept to the HF model of the machine, described in Section II-B. As can be seen, the HF magnetic model is formally similar to the fundamental one, so the HF active flux vector $\boldsymbol{\lambda}^{\mathrm{af,h}}$ can be defined as:

$$\boldsymbol{\lambda}^{\mathrm{af,h}} = \boldsymbol{\lambda}^{\mathrm{h}} - l_\mathrm{q}\boldsymbol{i}^{\mathrm{h}} \tag{11}$$

This expression can be applied in any reference frame. In particular, if written in rotor coordinates dq, and exploiting complex representation of vector quantities, (11) turns to be:

$$\begin{aligned}\boldsymbol{\lambda}^{\mathrm{af,h}} &= \lambda_\mathrm{d}^{\mathrm{h}} + j\lambda_\mathrm{q}^{\mathrm{h}} - l_\mathrm{q}\left(i_\mathrm{d}^{\mathrm{h}} + ji_\mathrm{q}^{\mathrm{h}}\right)\\ &= l_\mathrm{d} i_\mathrm{d}^{\mathrm{h}} + jl_\mathrm{q} i_\mathrm{q}^{\mathrm{h}} - l_\mathrm{q}\left(i_\mathrm{d}^{\mathrm{h}} + ji_\mathrm{q}^{\mathrm{h}}\right)\\ &= \left(l_\mathrm{d} - l_\mathrm{q}\right) i_\mathrm{d}^{\mathrm{h}}\end{aligned} \tag{12}$$

Therefore, the $\boldsymbol{\lambda}^{\mathrm{af,h}}$ vector lies on d axis. A visual representation of the extended HF-AF concept is depicted in Fig. 3(b).

IV. Proposed Sensorless Control

In this work, the proposed HF-AF concept is used for sensorless rotor position tracking at low speeds and standstill. The HF model of the machine is excited by injecting an HF voltage. All the quantities related to the HF injected signal will be represented with a subscript c, to be distinguished by the general HF component (superscript h).

A. Operating Principle

Despite the HF-AF concept is valid for any kind of HF signal, it was chosen to inject a sinusoidal pulsating voltage in the direction of the observed stator flux $\hat{d}_\mathrm{s}$, as depicted in Fig. 4. The $\hat{d}_\mathrm{s}, \hat{q}_\mathrm{s}$ coordinates are represented in Fig. 3(a). The phase shift between observed flux and α axis, i.e. the injection direction in $\alpha\beta$ frame, will be called θ_c, as shown in Fig. 3(b). In ideal conditions, i.e. perfect flux estimation, θ_c would be equal to the flux angle $\theta_\mathrm{c} = \theta_\mathrm{s} = \theta + \delta$.

It must be noted that, since the HF-AF concept is valid whatever the injection direction, eventual inaccuracy in determining $\hat{d}_\mathrm{s}$ does not affect the rotor position estimation.

Based on (5), the HF injected voltage corresponds to an HF flux:

$$\lambda_\mathrm{c} = \int u_\mathrm{c}\cos\left(\omega_\mathrm{c} t\right) = \frac{u_\mathrm{c}}{\omega_\mathrm{c}}\sin\left(\omega_\mathrm{c} t\right) \tag{13}$$

This HF flux is oriented in the same direction of the injected voltage:

$$\begin{cases} \lambda_\alpha^{\mathrm{h}} &= \lambda_\mathrm{c}\cos\theta_\mathrm{c} \\ \lambda_\beta^{\mathrm{h}} &= \lambda_\mathrm{c}\sin\theta_\mathrm{c} \end{cases} \tag{14}$$

In real dq coordinates, this expression turns to be:

$$\begin{cases} \lambda_\mathrm{d}^{\mathrm{h}} &= \lambda_\mathrm{c}\cos\left(\theta_\mathrm{c} - \theta\right) \\ \lambda_\mathrm{q}^{\mathrm{h}} &= \lambda_\mathrm{c}\sin\left(\theta_\mathrm{c} - \theta\right) \end{cases} \tag{15}$$

The HF current components can be retrieved from the HF magnetic model (7):

$$\begin{cases} i_\mathrm{d}^{\mathrm{h}} &= \frac{\lambda_\mathrm{d}^{\mathrm{h}}}{l_\mathrm{d}} &= \frac{\lambda_\mathrm{c}}{l_\mathrm{d}}\cos\left(\theta_\mathrm{c} - \theta\right) \\ i_\mathrm{q}^{\mathrm{h}} &= \frac{\lambda_\mathrm{q}^{\mathrm{h}}}{l_\mathrm{q}} &= \frac{\lambda_\mathrm{c}}{l_\mathrm{q}}\sin\left(\theta_\mathrm{c} - \theta\right) \end{cases} \tag{16}$$

The HF current components in stationary frame are obtained rotating (16) by the rotor position angle:

$$\begin{cases} i_\alpha^{\mathrm{h}} &= \lambda_\mathrm{c}\left(\frac{\cos(\theta_\mathrm{c}-\theta)}{l_\mathrm{d}}\cos\theta - \frac{\sin(\theta_\mathrm{c}-\theta)}{l_\mathrm{q}}\sin\theta\right) \\ i_\beta^{\mathrm{h}} &= \lambda_\mathrm{c}\left(\frac{\cos(\theta_\mathrm{c}-\theta)}{l_\mathrm{d}}\sin\theta + \frac{\sin(\theta_\mathrm{c}-\theta)}{l_\mathrm{q}}\cos\theta\right) \end{cases} \tag{17}$$

The HF components of AF in stationary reference frame are retrieved by using (14) and (17) into (11). For the α component, we have:

$$\lambda_\alpha^{\mathrm{af,h}} = \lambda_\mathrm{c}\left(\cos\theta_\mathrm{c} - \frac{l_\mathrm{q}}{l_\mathrm{d}}\cos\left(\theta_\mathrm{c} - \theta\right)\cos\theta + \sin\left(\theta_\mathrm{c} - \theta\right)\sin\theta\right) \tag{18}$$

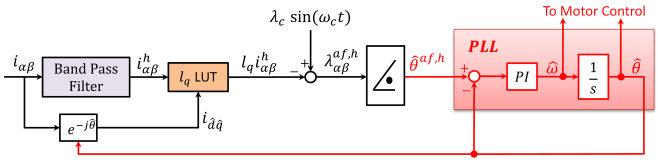

Fig. 5. Block diagram of the proposed position observer.

Similar expression can be obtained for the β component. After straightforward analytical manipulation, the following expression can be retrieved:

$$\begin{cases} \lambda_{\alpha}^{\mathrm{af,h}} = \lambda_{\mathrm{c}} \left(1 - \frac{l_{\mathrm{q}}}{l_{\mathrm{d}}}\right) \cos\left(\theta_{\mathrm{c}} - \theta\right) \cos\theta = |\boldsymbol{\lambda}^{\mathrm{af,h}}| \cos\theta \\ \lambda_{\beta}^{\mathrm{af,h}} = \lambda_{\mathrm{c}} \left(1 - \frac{l_{\mathrm{q}}}{l_{\mathrm{d}}}\right) \cos\left(\theta_{\mathrm{c}} - \theta\right) \sin\theta = |\boldsymbol{\lambda}^{\mathrm{af,h}}| \sin\theta \end{cases} \tag{19}$$

B. Direct Demodulation Process

As can be noted in (19), $\boldsymbol{\lambda}^{\mathrm{af,h}}$ is a pulsating vector shifted by an angle θ respect to the α axis. Therefore, the rotor position estimate can be directly obtained from the phase of $\boldsymbol{\lambda}^{\mathrm{af,h}}$. For taking into account the uncertainties inevitably introduced by the implementation (λ_{c} is estimated from the reference injected voltage, noise in current transducers and so on) this angle is indicated as $\hat{\theta}^{\mathrm{af,h}}$:

$$\begin{cases} \sin\hat{\theta}^{\mathrm{af,h}} = \frac{\lambda_{\beta}^{\mathrm{af,h}}}{|\boldsymbol{\lambda}^{\mathrm{af,h}}|} \\ \cos\hat{\theta}^{\mathrm{af,h}} = \frac{\lambda_{\alpha}^{\mathrm{af,h}}}{|\boldsymbol{\lambda}^{\mathrm{af,h}}|} \end{cases} \tag{20}$$

Similar to fundamental model, the estimated position $\hat{\theta}^{\mathrm{af,h}}$ can be either directly used or sent to a PLL. This second option was adopted in this paper, as depicted in Fig. 5, for better robustness at the cost of slightly limiting the position estimation bandwidth. The PLL extracts the observed position $\hat{\theta}$ and speed $\hat{\omega}$, used for motor control and flux observer.

The current components in stationary frame are first band-pass filtered and then multiplied by incremental inductance on q axis (l_{q}), coming from motor model (Fig. 5). The value of l_{q} is online updated to take into account the inductance variation depending on the working point.

It should be noted that it is not required to band-pass filter the observed flux, since its HF component can be accurately extracted from the reference HF voltage (13). Considering fairly good current measurement, the main uncertainty affecting position estimation is the knowledge of l_{q}, obtained from a manipulation of the machine flux maps. Anyway, if the flux maps are not available, they can be accurately retrieved from self-commissioning tests, e.g. [12]- [16]. It should also be considered that for SyR machines, the variability of l_{q} with the working point is moderate, except for very low i_{q}.

As seen, the proposed position observer is very simple with no requirement of low pass filters in tracking loop. This leads to possibility for enhancement of higher bandwidth of the speed loop.

TABLE I
RATINGS OF THE SYR MOTOR UNDER TEST.

Rated current [A]	2.8
Rated voltage [V]	408
Pole pairs	2
Rated torque [Nm]	7.1
Rated speed [rpm]	1479
Rated power [kW]	1.1
Phase resistance [Ω]	4.63
Switching frequency [kHz]	10

V. EXPERIMENTAL RESULTS

The effectiveness of proposed sensorless method is experimentally investigated in this section. Similar to [1], the motor control algorithm is based on Direct Flux Vector Control (DFVC). The adopted test rig is shown in Fig. 6, where the dSPACE1103, 1.1 kW synchronous reluctance motor, and inverter are highlighted. Both sampling and switching frequencies are fixed at 10 kHz. A variable speed dyno-drive was used to impose the load torque or shaft speed when the motor under test was sensorless speed or torque controlled respectively. The main motor data of the SyR prototype are report in Table I.

The results are presented for both torque and speed control modes at low speed and standstill.

A. Torque Control at Standstill and 20 rpm

Fig. 7 reports the results for torque control at standstill, where a nominal torque is stepwise applied to the motor at $t = 1.5\ s$ and then released at $t = 6.5\ s$. The figure depicts the observed torque, observed flux, three phase current, and position estimation error. As can be seen, $\Delta\theta$ is close to zero in both loaded and no load conditions.

The same test was repeated when the driving machine imposed a constant speed of 20 rpm, again applying nominal

Fig. 6. SyR motor under test (1.1 kW).

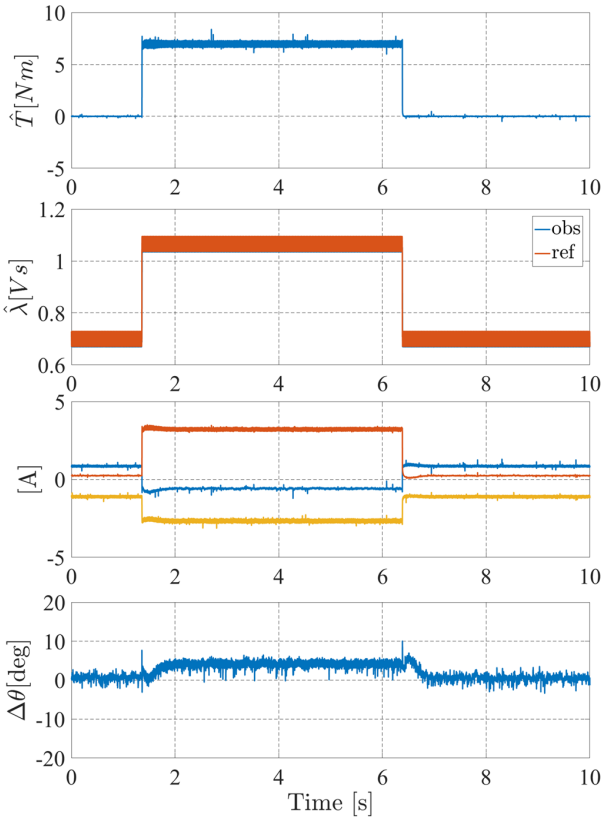

Fig. 7. Torque control at standstill with nominal torque.

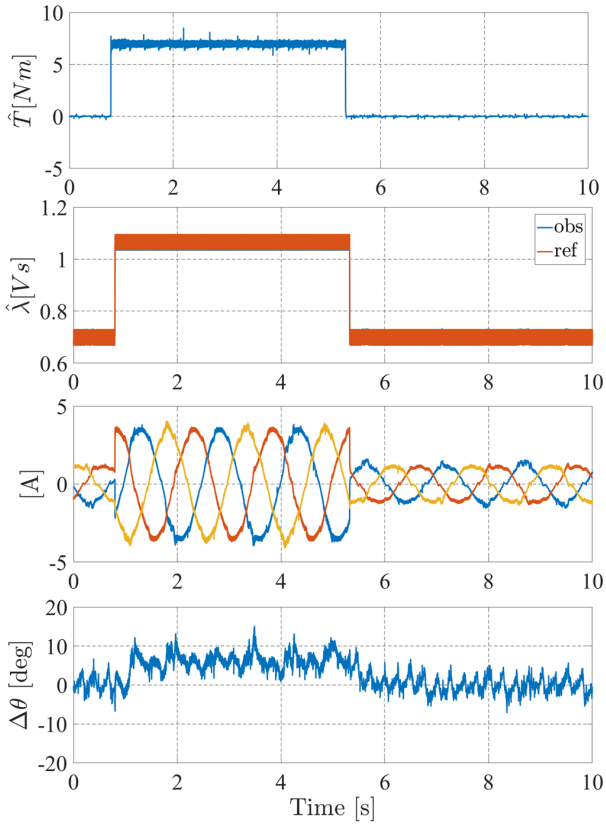

Fig. 8. Torque control at 20 rpm with nominal torque.

torque, as depicted in Fig. 8. Also in this case, the rotor position is properly estimated and $\Delta\theta$ remains close to zero even during torque transients.

B. Closed-Loop Speed Control

In Fig. 9 the motor under test was speed controlled with 0 rpm reference speed. The rated load torque is applied and released by the driving machine. The Figure presents estimated and actual speed, observed torque, three phase currents, and estimated position error. Also in this case, $\Delta\theta$ is very close to zero and dynamic response of the system is good.

Finally, Fig. 10 illustrates a speed transient test at no load, where the rotor speed reference moves from standstill to 50 rpm following a sharp ramp, and then it decelerates to standstill. As can bee seen, also in this test the position estimation error is close to zero in steady state and transients, and the dynamic response is fast and accurate.

VI. Conclusion

This paper proposes a generalized formulation for active flux concept. In turn, the HF component of the active flux vector was defined, analytically retrieved and adopted for implementing a robust and reliable sensorless control exploiting HF voltage injection. If the traditional AF algorithms can only be adopted at medium-high speed, the proposed technique extends the operating area down to low speed and standstill conditions. In addition, the proposed HF-AF method is compatible with direct demodulation, intended as direct calculation of sine and cosine of estimated HF-AF flux components. This avoid the additional LPF normally associated to HF components demodulation, permitting fast dynamic performances and accurate position estimation both in steady state and transient conditions, when the motor was torque or speed controlled. Several experimental results prove the consistency of the proposed sensorless technique.

References

[1] A. Yousefi-Talouki, P. Pescetto, G. Pellegrino and I. Boldea, "Combined Active Flux and High-Frequency Injection Methods for Sensorless Direct-Flux Vector Control of Synchronous Reluctance Machines," in IEEE Transactions on Power Electronics, vol. 33, no. 3, pp. 2447-2457, March 2018.

[2] A. Yousefi-Talouki, P. Pescetto and G. Pellegrino, "Sensorless Direct Flux Vector Control of Synchronous Reluctance Motors Including Standstill, MTPA, and Flux Weakening," in IEEE Transactions on Industry Applications, vol. 53, no. 4, pp. 3598-3608, July-Aug. 2017.

[3] T. Tuovinen and M. Hinkkanen, "Adaptive Full-Order Observer With High-Frequency Signal Injection for Synchronous Reluctance Motor Drives," in IEEE Journal of Emerging and Selected Topics in Power Electronics, vol. 2, no. 2, pp. 181-189, June 2014

[4] Zhiqian Chen, M. Tomita, S. Doki and S. Okuma, "An extended electromotive force model for sensorless control of interior permanent-magnet synchronous motors," in IEEE Transactions on Industrial Electronics, vol. 50, no. 2, pp. 288-295, April 2003.

[5] F. Briz and M. W. Degner, "Rotor Position Estimation," in IEEE Industrial Electronics Magazine, vol. 5, no. 2, pp. 24-36, June 2011.

[6] D. Paulus, P. Landsmann and R. Kennel, "Sensorless field- oriented control for permanent magnet synchronous machines with an arbitrary

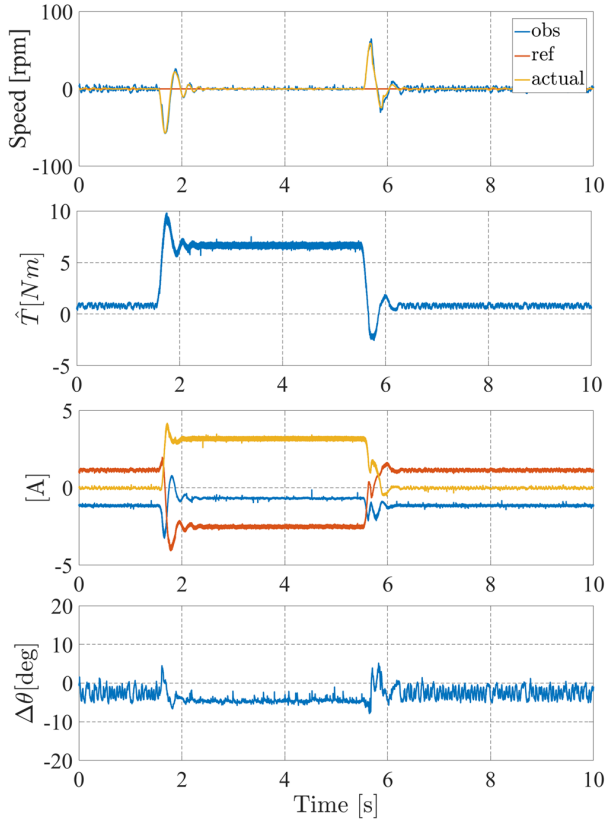

Fig. 9. Speed control test at standstill with step nominal loading.

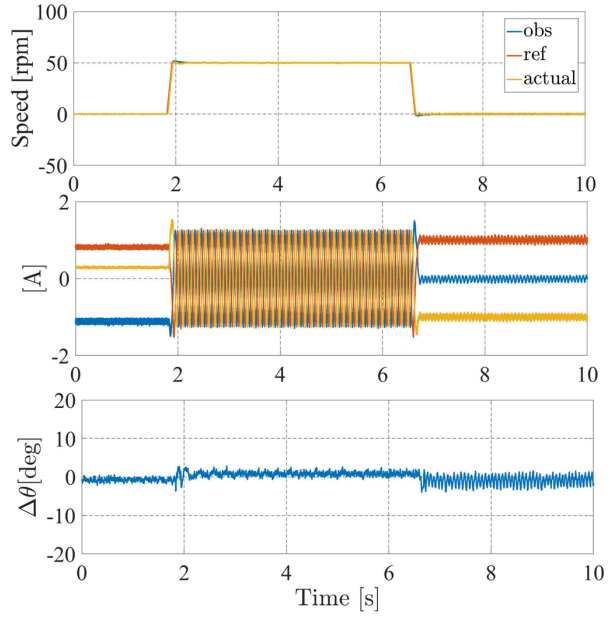

Fig. 10. No load speed control test.

injection scheme and direct angle calculation," 2011 Symposium on Sensorless Control for Electrical Drives, Birmingham, 2011, pp. 41-46.

[7] S. Bolognani, S. Calligaro, R. Petrella and M. Tursini, "Sensorless Control of IPM Motors in the Low-Speed Range and at Standstill by HF Injection and DFT Processing," in IEEE Transactions on Industry Applications, vol. 47, no. 1, pp. 96-104, Jan.-Feb. 2011.

[8] F. J. W. Barnard, W. T. Villet and M. J. Kamper, "Hybrid Active-Flux and Arbitrary Injection Position Sensorless Control of Reluctance Synchronous Machines," in IEEE Transactions on Industry Applications, vol. 51, no. 5, pp. 3899-3906, Sept.-Oct. 2015.

[9] S. Agarlita, I. Boldea and F. Blaabjerg, "High-Frequency-Injection-Assisted "Active-Flux"-Based Sensorless Vector Control of Reluctance Synchronous Motors, With Experiments From Zero Speed," in IEEE Transactions on Industry Applications, vol. 48, no. 6, pp. 1931-1939, Nov.-Dec. 2012.

[10] I. Boldea, M. C. Paicu and G. Andreescu, "Active Flux Concept for Motion-Sensorless Unified AC Drives," in IEEE Transactions on Power Electronics, vol. 23, no. 5, pp. 2612-2618, Sept. 2008.

[11] M. Tursini, M. Villani, G. Fabri, S. Paolini, A. Credo and A. Fioravanti, "Sensorless control of a synchronous reluctance motor by finite elements model results," 2017 IEEE International Symposium on Sensorless Control for Electrical Drives (SLED), Catania, 2017, pp. 19-24

[12] S. A. Odhano, P. Pescetto, H. A. A. Awan, M. Hinkkanen, G. Pellegrino and R. Bojoi, "Parameter Identification and Self-Commissioning in AC Motor Drives: A Technology Status Review," in IEEE Transactions on Power Electronics, vol. 34, no. 4, pp. 3603-3614, April 2019.

[13] Y. Gao, R. Qu, Yu Chen, Jian Li and Wei Xu, "Review of off-line synchronous inductance measurement method for permanent magnet synchronous machines," 2014 IEEE Conference and Expo Transportation Electrification Asia-Pacific (ITEC Asia-Pacific), Beijing, 2014, pp. 1-6.

[14] L. Peretti, P. Sandulescu and G. Zanuso, "Self-commissioning of flux linkage curves of synchronous reluctance machines in quasi-standstill condition," in IET Electric Power Applications, vol. 9, no. 9, pp. 642-651, 11 2015.

[15] M. Hinkkanen, P. Pescetto, E. Mölsä, S. E. Saarakkala, G. Pellegrino and R. Bojoi, "Sensorless Self-Commissioning of Synchronous Reluctance Motors at Standstill Without Rotor Locking," in IEEE Transactions on Industry Applications, vol. 53, no. 3, pp. 2120-2129, May-June 2017.

[16] P. Pescetto and G. Pellegrino, "Automatic Tuning for Sensorless Commissioning of Synchronous Reluctance Machines Augmented With High-Frequency Voltage Injection," in IEEE Transactions on Industry Applications, vol. 54, no. 5, pp. 4485-4493, Sept.-Oct. 2018.